Anisotropic Transport and Magnetic Properties of Ternary Uranium Antimonides U_3ScSb_5 and U_3TiSb_5

Arthur Mar*

Department of Chemistry, University of Alberta, Edmonton, Alberta, Canada T6G 2G2

Olivier Tougait, Michel Potel, and Henri Noël

Sciences chimiques de Rennes, UMR CNRS 6226, Université de Rennes 1, Avenue du Général Leclerc, 35042 Rennes, France

Elsa B. Lopes

Dep. Química/CFMC Instituto Tecnológico e Nuclear, Estrada Nacional 10, P-2686-953 Sacavém, Portugal

Received June 1, 2006. Revised Manuscript Received June 28, 2006

Single needle-shaped crystals of U_3ScSb_5 and U_3TiSb_5 were grown in a tin flux. The structure of the new compound U_3ScSb_5 was determined from single-crystal X-ray diffraction data (Pearson symbol *hP*18, hexagonal, space group $P6_3/mcm$, $Z = 2$, $a = 9.2145(2)$ Å, $c = 6.1938(2)$ Å). The angular dependence of the magnetization has been studied. Ferromagnetic ordering develops within the *ab* plane at $T_C = 130$ K for U_3ScSb_5 and 160 K for U_3TiSb_5, but there are essentially no magnetic interactions parallel to the *c* axis, confirming the high anisotropy expected from the crystal structure. In both cases, the easy axis for magnetization is the [120] direction. A sharp decrease below the ordering temperature is observed in the electrical resistivity parallel to the *c* axis; in contrast, the temperature dependence is much weaker within the *ab* plane. For U_3TiSb_5, a second transition occurs at 25 K, possibly arising from a spin reorientation process. The thermoelectric power measured along the *c* axis for both compounds is positive and small at high temperatures, following approximately a linear dependence with temperature indicative of metallic behavior in this region. The thermopower exhibits a kink at the ferromagnetic transition temperature in the case of U_3TiSb_5, but it is not so clear in the case of U_3ScSb_5. A change in sign of the thermopower occurs below T_C for both compounds, characteristic of multiband conducting systems.

Introduction

The stuffed Mn_5Si_3-type structure, also known as the Hf_5Cu_3Sn-type structure, is adopted by an extensive family of polar intermetallic compounds that has long been popularized by Corbett.[1,2] For example, compounds such as La_5Sb_3Br can be considered to be formed by filling empty sites within the hexagonal host structure La_5Sb_3 by interstitial Br atoms.[3] Indeed, some binary phases such as U_5Sb_4 may also be derived in this manner, in which Sb atoms enter a hypothetical "U_5Sb_3" host structure; in these cases, the structure is known as a Ti_5Ga_4-type.[4] Less familiar are the antitype variants. These include U_3MSb_5 (M = Ti, Zr, Hf, V, Nb, Ta, Cr, Mn),[5,6] R_3MSb_5 (R = rare earth; M = Ti, Zr, Hf, Nb),[7,8] U_3TiX_5 (X = Ge, Sn),[9] Ce_3MnBi_5,[10] and La_3MgBi_5.[11] The host structures do not actually exist except in a formal sense (U_3Sb_5, R_3Sb_5, R_3Bi_5, or U_3Sn_5) or with a different structure type (U_3Ge_5 is a defect AlB_2-type derivative).[12]

Although measurements are still scarce, the properties of some of these hexagonal stuffed Mn_5Si_3-type phases are expected to be highly anisotropic, reflecting their crystal structure. U_5Sb_4 itself orders ferromagnetically along *c*.[4] U_3TiGe_5 has a ferromagnetic component along *c* and an antiferromagnetic triangular component within the *ab* plane.[9] U_3MSb_5 (M = Zr, Hf, Nb) and U_3TiSn_5 also order ferromagnetically, but their anisotropy was not determined owing to the unavailability of suitable single crystals.[6,9] The properties of the prototype compound, U_3TiSb_5, have not yet been investigated.[5]

* To whom correspondence should be addressed. E-mail: arthur.mar@ualberta.ca.

(1) Corbett, J. D.; Garcia, E.; Guloy, A. M.; Hurng, W.-M.; Kwon, Y.-U.; Leon-Escamilla, E. A. *Chem. Mater.* **1998**, *10*, 2824−2836.
(2) Corbett, J. D. *Inorg. Chem.* **2000**, *39*, 5178−5191.
(3) Jensen, E. A.; Hoistad, L. M.; Corbett, J. D. *J. Solid State Chem.* **1999**, *144*, 175−180.
(4) Paixão, J. A.; Rebizant, J.; Blaise, A.; Delapalme, A.; Sanchez, J. P.; Lander, G. H.; Nakotte, H.; Burlet, P.; Bonnet, M. *Physica B* **1994**, *203*, 137−146.
(5) Brylak, M.; Jeitschko, W. *Z. Naturforsch., B: Chem. Sci.* **1994**, *49*, 747−752.
(6) Tkachuk, A. V.; Muirhead, C. P. T.; Mar, A. *J. Alloys Compd.* **2006**, *418*, 39−44.
(7) Ferguson, M. J.; Hushagen, R. W.; Mar, A. *J. Alloys Compd.* **1997**, *249*, 191−198.
(8) Moore, S. H. D.; Deakin, L.; Ferguson, M. J.; Mar, A. *Chem. Mater.* **2002**, *14*, 4867−4873.
(9) Boulet, P.; Gross, G. M.; André, G.; Bourée, F.; Noël, H. *J. Solid State Chem.* **1999**, *144*, 311−317.
(10) Pecharsky, A. O.; Gschneidner, K. A., Jr. *J. Alloys Compd.* **1999**, *287*, 67−70.
(11) Pan, D.-C., Sun, Z.-M.; Mao, J.-G. *J. Solid State Chem.* **2006**, *179*, 1016−1021.
(12) Boulet, P.; Potel, M.; André, G.; Rogl, P.; Noël, H. *J. Alloys Compd.* **1999**, *283*, 41−44.

10.1021/cm061281y CCC: $33.50
Published on Web 08/04/2006

In materials of tetragonal or hexagonal symmetry where crystalline electric field (CEF) effects are strong, the magnetic moments will be aligned either axially or within the basal plane. There has been considerable progress in the analysis of magnetic anisotropy in a variety of tetragonal materials, such as RNi_2Ge_2, $DyAgSb_2$, $CeMSb_2$ (M = Cu, Au, Ni), and $Lu(Ni_{1-x}Co_x)_2B_2C$, where detailed measurements of the angular-dependent magnetization have been made.[13−16] Relatively less has been done in the case of hexagonal materials, such as *R*AgGe and *R*PtIn, which are antiferromagnetic and undergo metamagnetic transitions.[17−20] To our knowledge, no similar studies have been conducted on uranium intermetallics.

Given the unanswered questions about the nature of the anisotropy and the incomplete characterization of the U_3MSb_5 compounds, we have endeavoured to prepare suitable specimens for further property measurements. We report here the first studies of the electrical transport and magnetic properties of U_3TiSb_5 and the new compound U_3ScSb_5, measured along *c* and within the *ab* plane on large single crystals.

Experimental Section

Synthesis. Starting materials were U turnings (nuclear grade), Sc turnings (99.9%, Strem), Ti dendritic pieces (99.99%, Strem), Sb shot (99.999%, Strem), and Sn rod (99.9999%, Prolabo). U_3ScSb_5 and U_3TiSb_5 were prepared by reaction of stoichiometric mixtures of the elements on a 0.5-g scale, in the presence of 3.5 g of Sn, in cylindrical alumina crucibles within evacuated fused-silica tubes. The tubes were placed in a vertical furnace, which was programmed to heat at 1000 °C for 10 h and then to slowly cool to 800 °C at a rate of 2 °C/h and to 600 °C at a rate of 5 °C/h. The tubes were removed when the furnace had cooled to approximately 700 °C. The Sn flux was removed by treatment with dilute (1:1) hydrochloric acid, and the resulting crystals were washed plentifully with distilled water. These crystals are needle-shaped and have hexagonal cross sections. Energy-dispersive X-ray (EDX) analyses on a 6400-JSM scanning electron microscope equipped with an Oxford Link Isis spectrometer revealed the presence of all three elements with atomic percentages averaged over several crystals (U_3ScSb_5, 32(2)% U, 10(1)% Sc, 58(2)% Sb; U_3TiSb_5, 34(2)% U, 12(1)% Ti, 54(2)% Sb) that are in good agreement with the ideal composition (33% U, 11% *M*, 56% Sb). The presence of Sn was not detected in these crystals. Moreover, the good agreement of the cell parameters of arc-melted samples (prepared in the absence of Sn) and of flux-grown crystals supports these elemental compositions.

Structure Determination. Intensity data for U_3ScSb_5 were collected on a Nonius Kappa CCD diffractometer at 20 °C, with a complete strategy for filling more than a hemisphere calculated with use of the program COLLECT.[21] The data were processed with the program DENZO in the Kappa CCD software package.[21] Numerical absorption corrections were applied with the program ANALYTICAL.[22] The structure was refined with use of the program SHELXL-97.[23] The centrosymmetric space group $P6_3/mcm$ was chosen, and initial atomic positions were found by direct methods, which confirmed that the anti-Hf_5Sn_3Cu-type structure was adopted. Refinements proceeded in a straightforward manner. In particular, refinements on the occupancy factors confirmed that all sites are fully occupied and have reasonable displacement parameters.

Table 1. Crystallographic Data for U_3ScSb_5

formula	U_3ScSb_5
formula mass (amu)	1367.80
space group	$P6_3/mcm$ (No. 193)
a (Å)	9.2145(2)
c (Å)	6.1938(2)
V (Å^3)	455.44(2)
Z	2
ρ_{calcd} (g cm^{-3})	9.974
crystal dimensions (mm)	0.07 × 0.04 × 0.03
radiation (λ, Å)	graphite-monochromated Mo Kα (0.710 73)
μ(Mo Kα) (cm^{-1})	683.12
transmission factors	0.055−0.186
2θ limits (deg)	8.84 ≤ 2θ(Mo Kα) ≤ 80.00
data collected	$-16 \le h \le 12$, $-16 \le k \le 15$, $-10 \le l \le 11$
no. of data collcd	9117
no. of unique data, including $F_o^2 < 0$	546
no. of unique data, with $F_o^2 > 2\sigma(F_o^2)$	506
no. of variables	14
$R(F)$ for $F_o^2 > 2\sigma(F_o^2)$[a]	0.029
$R_w(F_o^2)$[b]	0.070
goodness of fit	1.07
$(\Delta\rho)_{max}$, $(\Delta\rho)_{min}$ (e Å^{-3})	5.06, −3.29

[a] $R(F) = \Sigma||F_o| - |F_c||/\Sigma|F_o|$. [b] $R_w(F_o^2) = [\Sigma[w(F_o^2 - F_c^2)^2]/\Sigma wF_o^4]^{1/2}$; $w^{-1} = [\sigma^2(F_o^2) + (Ap)^2 + Bp]$, where $p = [\max(F_o^2,0) + 2F_c^2]/3$.

Table 2. Positional and Equivalent Isotropic Displacement Parameters for U_3ScSb_5

atom	Wyckoff posn	x	y	z	U_{eq} (Å^2)[a]
U	6*g*	0.61557(4)	0	1/4	0.0087(1)
Sc	2*b*	0	0	0	0.0098(4)
Sb1	6*g*	0.26849(6)	0	1/4	0.0083(1)
Sb2	4*d*	1/3	2/3	0	0.0084(1)

[a] U_{eq} is defined as one-third of the trace of the orthogonalized $\mathbf{U}_{ij}$ tensor.

Table 3. Selected Interatomic Distances (Å) in U_3ScSb_5

U−Sb1 (×2)	3.1472(3)	U−U (×2)	3.7586(4)
U−Sb1	3.1982(7)	M−Sb1 (×6)	2.9186(5)
U−Sb2 (×4)	3.2569(1)	M−M (×2)	3.0969(2)
U−Sb1 (×2)	3.2760(2)	Sb2−Sb2 (×2)	3.0969(2)

Crystal data and further details of the data collection are given in Table 1. Final values of the positional and displacement parameters are given in Table 2. Interatomic distances are listed in Table 3. Further data, in the form of a CIF, have been sent to Fachinformationszentrum Karlsruhe, Abt. PROKA, 76344 Eggenstein-Leopoldshafen, Germany, as supporting information No. CSD-416734 and can be obtained by contacting FIZ (quoting the article details and the corresponding CSD numbers).

(13) Bud'ko, S. L.; Islam, Z.; Wiener, T. A.; Fisher, I. R.; Lacerda, A. H.; Canfield, P. C. *J. Magn. Magn. Mater.* **1999**, *205*, 53−78.
(14) Myers, K. D.; Canfield, P. C.; Kalatsky, V. A.; Pokrovsky, V. L. *Phys. Rev. B* **1999**, *59*, 1121−1128.
(15) Thamizhavel, A.; Takeuchi, T.; Okubo, T.; Yamada, M.; Asai, R.; Kirita, S.; Galatanu, A.; Yamamoto, E.; Ebihara, T.; Inada, Y.; Settai, R.; Ōnuki, Y. *Phys. Rev. B* **2003**, *68*, 054227−1−054227−8.
(16) Kogan, V. G.; Bud'ko, S. L.; Canfield, P. C.; Miranović, P. *Phys. Rev. B* **1999**, *60*, R12577−R12580.
(17) Baran, S.; Hofmann, M.; Leciejewicz, J.; Penc, B.; Ślaski, M.; Szytuła, A. *J. Alloys Compd.* **1998**, *281*, 92−98.
(18) Morosan, E.; Bud'ko, S. L.; Canfield, P. C.; Torikachvili, M. S.; Lacerda, A. H. *J. Magn. Magn. Mater.* **2004**, *277*, 298−321.
(19) Morosan, E.; Bud'ko, S. L.; Canfield, P. C. *Phys. Rev. B* **2005**, *71*, 014445-1−014445-20.
(20) Morosan, E.; Bud'ko, S. L.; Canfield, P. C. *Phys. Rev. B* **2005**, *72*, 014425-1−014425-16.
(21) *Kappa CCD Program Package*; Nonius BV: Delft, The Netherlands, 1998.
(22) de Meulenaer, J.; Tompa, H. *Acta Crystallogr., Sect. A* **1965**, *19*, 1014−1018.
(23) Sheldrick, G. M. *SHELXL-97*; University of Göttingen: Göttingen, Germany, 1997.

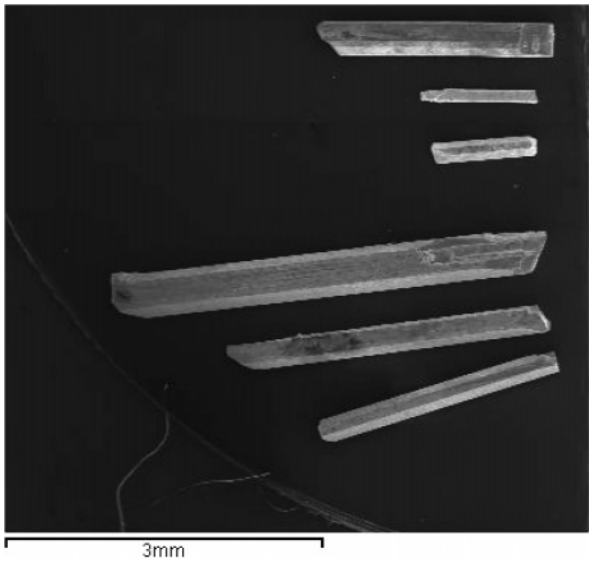

Figure 1. Single crystals of U_3ScSb_5 (upper three) and U_3TiSb_5 (lower three). The needle axis corresponds to the crystallographic *c* axis.

The cell parameters refined from a single crystal of U_3TiSb_5 (a = 9.139(1) Å, c = 6.100(1) Å) agree well with those reported previously (a = 9.139(2) Å, c = 6.112(2) Å).[5]

Property Measurements. Measurements of dc magnetic susceptibility were made on a 2.5-mg crystal of U_3ScSb_5 and a 1.3-mg crystal of U_3TiSb_5 using a Quantum Design MPMS SQUID magnetometer at temperatures between 2 and 300 K and under applied magnetic fields up to 5 T. The angular-dependent magnetization was measured by mounting the crystal on a horizontal rotator with the needle axis aligned either parallel or perpendicular with the applied field. Because the samples are strongly ferromagnetic, they were secured by a cryogenic varnish.

The electrical resistivity was measured on single crystals of U_3ScSb_5 and U_3TiSb_5 between 2 and 300 K by standard four-probe techniques on a Quantum Design PPMS system equipped with an ac transport controller (model 7100), with a current of 100 μA and a frequency of 16 Hz. The resistivity was first measured along the needle axis of the crystal, which corresponds to the crystallographic *c* axis (ρ_c). The crystals were then truncated and reoriented with the electrical leads mounted in an arrangement to measure the resistivity within the *ab* plane (ρ_{ab}).

The thermopower was measured relative to gold by a slow ac technique (10^{-2} Hz) in an apparatus similar to one described previously.[24] The thermal gradient applied along the *c* axis was on the order of 1 K.

Results

Structure. Crystals of the U_3MSb_5 series, previously known for M = Ti, Zr, Hf, V, Nb, Ta, Cr, and Mn[5,6] and now extended to include M = Sc, are characterized by their acicular habits with hexagonal cross sections (Figure 1). The shape reflects their hexagonal crystal structure, an anti-Hf_5Cu_3Sn-type. Ninefold-coordinate U atoms in tricapped trigonal prismatic geometry separate confacial chains of metal-centered octahedra and skewers of Sb atoms aligned along the *c* direction (Figure 2). Although there are still not as many representatives as the normal type, this inverse structure type may prove to be just as versatile, not only through substitution with different *M* but also through replacement of U by rare earths or Sb by other p-block elements. Because of the considerable covalent character of bonds to U and the greater radial extension of 5f orbitals, it is not obvious that the electronic structure is as anisotropic as suggested by Figure 2, compared to the rare-earth analogues R_3MSb_5.[7,8] The new compound U_3ScSb_5 is noteworthy in being the most electron-poor of the U_3MSb_5 series and in having the most expanded structure, with the longest interatomic distances.

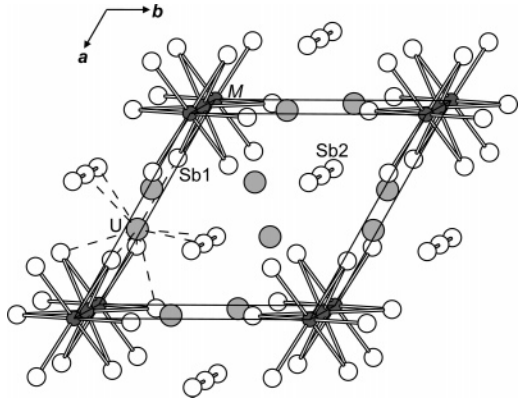

Figure 2. Structure of U_3MSb_5 (M = Sc, Ti) viewed down the *c* direction. The large lightly shaded circles are U atoms, the small solid circles are *M* atoms, and the medium open circles are Sb atoms.

Magnetic Properties. The availability of large single crystals presents a good opportunity to study the magnetic behavior of U_3ScSb_5 and U_3TiSb_5 as a function of orientation. Because these compounds were found to be strongly magnetic, the magnetization of an individual crystal (<2.5 mg) was still easily measured within the detection limits of the magnetometer. In the discussion below, the axis of rotation is always disposed horizontally and the applied field is oriented vertically.

U_3ScSb_5. To ascertain whether U_3ScSb_5 magnetizes preferentially along the axial direction (*c*) or within the basal plane (*ab*), the needle axis of the crystal was first rotated relative to the applied field. On the assumption that U_3ScSb_5 would behave similarly to previously measured U_3MX_5 compounds, which order ferromagnetically at moderate temperatures (ranging from 65 K for U_3TiSn_5[9] to 141 K for U_3HfSb_5[6]), the magnetization was measured at 10 K. Figure 3a shows the angular dependence of the magnetization over a 180° range. The magnetization reaches its maximum at θ = 90°, when *c* is normal to the applied field, and essentially vanishes at θ = 0°, when *c* is parallel to the applied field. This observation implies that the moments are largely confined to the *ab* plane. The angular dependence can be fit to a simple sinusoidal function, shown as the solid line. In a similar experiment on tetragonal $(Tb_{0.2}Lu_{0.98})Ni_2Ge_2$, the appearance of cusps at 180° intervals signaled saturation behavior.[13] The absence of these cusps in Figure 3a indicates that saturation has not yet been reached at 1000 Oe.

The temperature dependence of the dc magnetic susceptibility, under an applied field of 5000 Oe, was measured with the crystal in either of the two orientations, θ = 90° or θ = 0° (Figure 3b). The susceptibility increases rapidly below ~150 K for θ = 90°, but it remains low at all temperatures for θ = 0°. The inverse susceptibility in the high-temperature

(24) Chaikin, P. M.; Kwak, J. F. *Rev. Sci. Instrum.* **1975**, *46*, 218−220.

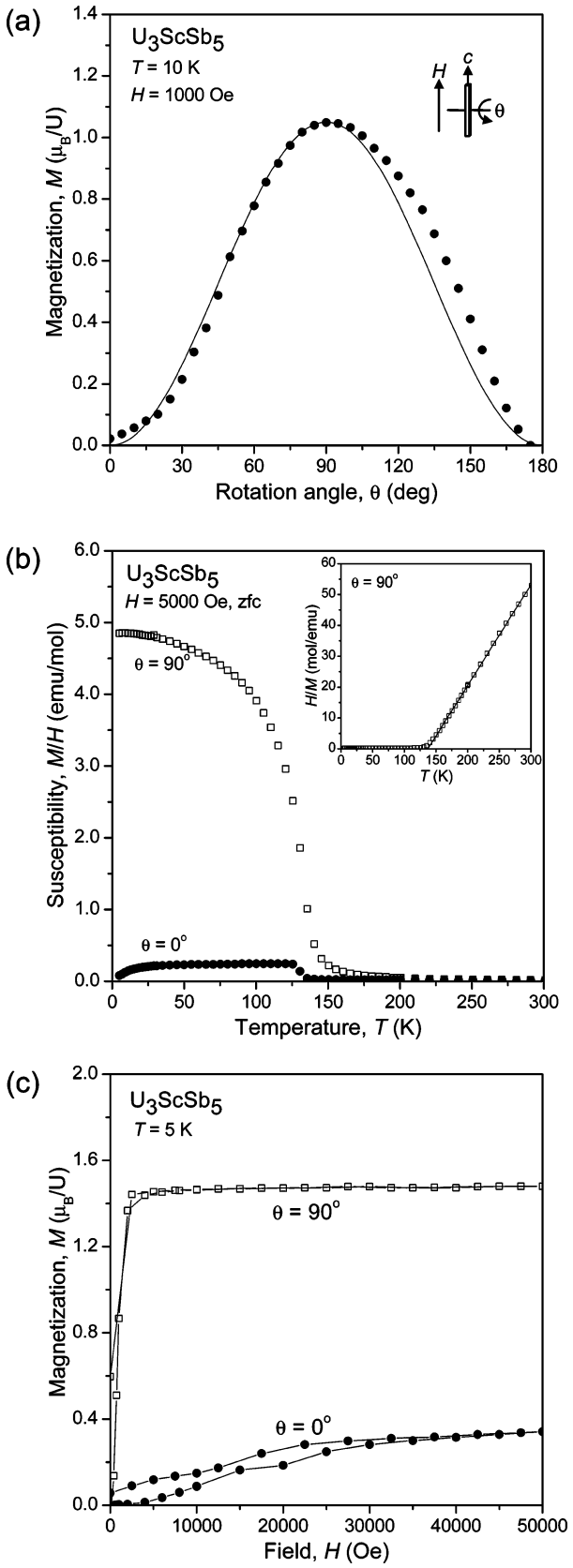

Figure 3. Magnetic properties of a single crystal of U_3ScSb_5 with the needle axis *c* rotated with respect to the applied field *H*. (a) Angular dependence of the magnetization at 10 K and 1000 Oe in the range $0 < \theta < 180°$. At $\theta = 0°$, $H \parallel c$ and at $\theta = 90°$, $H \perp c$. The solid line is a fit to the experimental data by a sinusoidal function. (b) Temperature dependence of the zero-field-cooled magnetic susceptibility at $\theta = 0°$ and $\theta = 90°$. The inset shows a fit of the inverse susceptibility data at $\theta = 90°$ to the Curie−Weiss law. (c) Field dependence of the magnetization at $\theta = 0°$ and $\theta = 90°$, at 5 K.

regime (150−300 K) for $\theta = 90°$ (inset of Figure 3b) follows the Curie−Weiss law, $\chi = C/(T - \theta_p)$, with parameters $C = 3.06(1)$ (emu·K)/mol and $\theta_p = 137(1)$ K, indicative of ferromagnetic coupling. The effective magnetic moment calculated from the Curie constant is thus $\mu_{eff} = 2.86\ \mu_B$/U for $H \perp c$. Isothermal magnetization curves at 5 K are shown in Figure 3c. For $\theta = 90°$, the magnetization saturates quickly to $M_s = 1.5\ \mu_B$/U. Although this value of the saturation moment is much lower than expected for U^{3+} or U^{4+} ions calculated using the spin−orbit coupling scheme, it agrees well with those reported for ferromagnetic U compounds[4,25] or the value of the magnetic moments found by neutron diffraction experiments.[26,27] The hysteresis is only slight, with a remanent magnetization of $M_{rem} = 0.6\ \mu_B$/U. In contrast, for $\theta = 0°$, the magnetization increases only slowly and linearly with field. These observations clearly establish a model of a rather soft and highly anisotropic ferromagnet that orders entirely within the *ab* plane and with essentially no magnetic interactions along the *c* direction. The slight discrepancy in magnetization between the experimental data and the sinusoidal curve (Figure 3a) may be attributed to a small torsional drift in the Cu wire that conveys the rotation to the sample. The small increase in susceptibility below ~150 K in the $\theta = 0°$ curve (Figure 3b) likely arises from a small error in crystal alignment on the horizontal rotator.

The same crystal was next remounted on the horizontal rotator with its needle axis oriented perpendicular to the applied field. Figure 4a shows the angular dependence of the magnetization at 10 K over a 180° range under an applied field of 5000 Oe, where the saturated state has been attained. The magnetization displays cusps with a periodicity of 60°, consistent with the hexagonal symmetry within the *ab* plane. Within these 60° intervals, the curve can be fit to a simple sinusoidal function, with deviations presumably arising from slight misalignment of the crystal. The magnetization reaches a maximum when *H* is normal to the (100) faces (at $\phi = 0°$, 60°, ...) and a minimum when *H* bisects them (at $\phi = 30°$, 90°, ...), implying that the magnetic moments are aligned parallel to the [120] direction (and its symmetry equivalents) in the saturated state. This behavior is similar to that seen in hexagonal TmAgGe, except that the locations of minima and maxima are reversed (notwithstanding the erroneous labeling of directions in the reference).[18] A simple trigonometric analysis based on a model of three superposed coplanar Ising systems in TmAgGe gives a calculated ratio of $\cos 30° = 0.866$ for the minimum-to-maximum magnetization.[18] For U_3ScSb_5, the observed ratio (from the curve fitting) is 1.32/1.52 = 0.868, fortuitously very close to the expected value.

With the crystal set in the $\phi = 0°$ orientation, the magnetization was measured under a low applied field of 500 Oe, with the zero-field-cooled and field-cooled curves deviating below an irreversibility temperature near 80 K (Figure 4b). The Curie temperature was located from a plot of $d\chi/dT$, which reveals a sharp transition at $T_C = 130$ K

(25) Vogt, O.; Mattenberger, K. *J. Magn. Magn. Mater.* **2003**, *261*, 244−256.
(26) Boulet, P.; Daoudi, A.; Potel, M.; Noël, H.; Gross, G. M.; André, G.; Bourée, F. *J. Alloys Compd.* **1997**, *247*, 104−108.
(27) Pechev, S.; Chevalier, B.; Laffargue, D.; Darriet, B.; Etourneau, J. *J. Alloys Compd.* **1998**, *271−273*, 448−451.

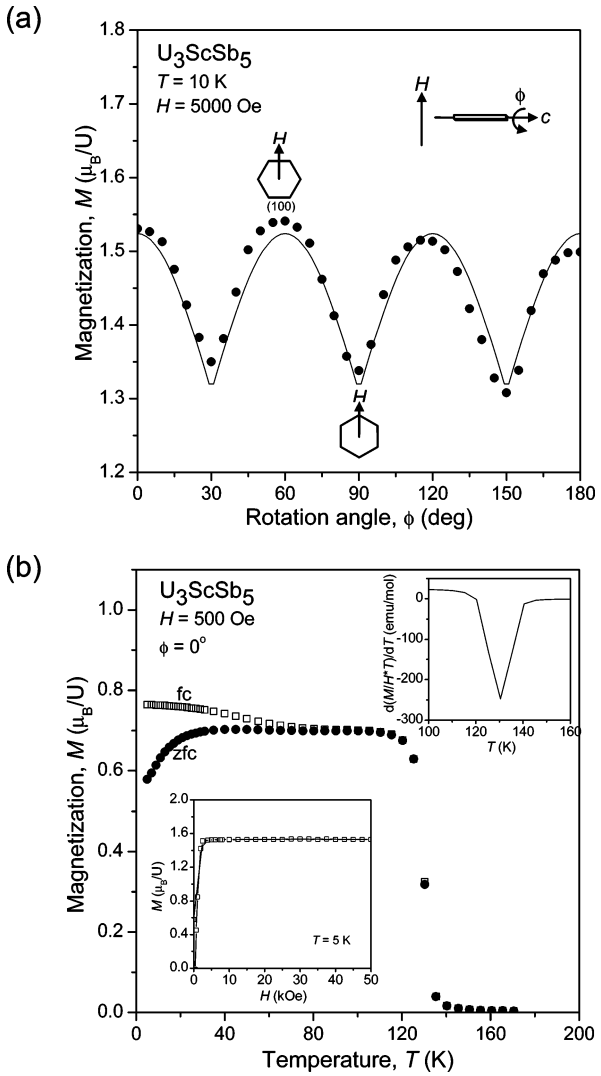

Figure 4. Magnetic properties of a single crystal of U_3ScSb_5 rotated about its needle axis *c*, oriented normal to the applied field *H*. (a) Angular dependence of the magnetization within the *ab* plane at 10 K and 5000 Oe in the range $0 < \phi < 180°$. The solid line is a fit to the experimental data by a sinusoidal function within 60° intervals. (b) Temperature dependence of field-cooled and zero-field-cooled magnetization under a low applied field of $H = 500$ Oe at $\phi = 0°$. The Curie temperature is determined from the plot of the derivative of $(M/H)T$, shown in the upper inset. The isothermal magnetization at 5 K is shown in the lower inset.

(upper inset). The isothermal magnetization at 5 K (lower inset) has a saturation value of $M_S = 1.53\ \mu_B$/U, close to that found earlier (Figure 3c), implying that the crystal was coincidentally mounted near $\phi = 0°$ when $\theta = 90°$ in the previous experiment.

U_3TiSb_5. Figure 5a shows the magnetization of a single crystal of U_3TiSb_5 with its needle axis rotated relative to the applied field over the full 360° range at 10 K. Again, the curves show the expected periodicity and anisotropy, with the cusp features becoming more pronounced as the applied field is increased. At 5000 Oe, the cusps are well-defined, implying that saturation has been reached by this point. Figure 5b shows the temperature dependence of the zero-field-cooled susceptibility under 5000 Oe at two orientations of the crystal, revealing the extreme magnetic anisotropy of strong ferromagnetism confined entirely within the *ab* plane. A fit of the inverse in-plane susceptibility ($\theta = 90°$) to the Curie−Weiss law (inset) gives $C = 2.97(2)$ (emu·K)/mol

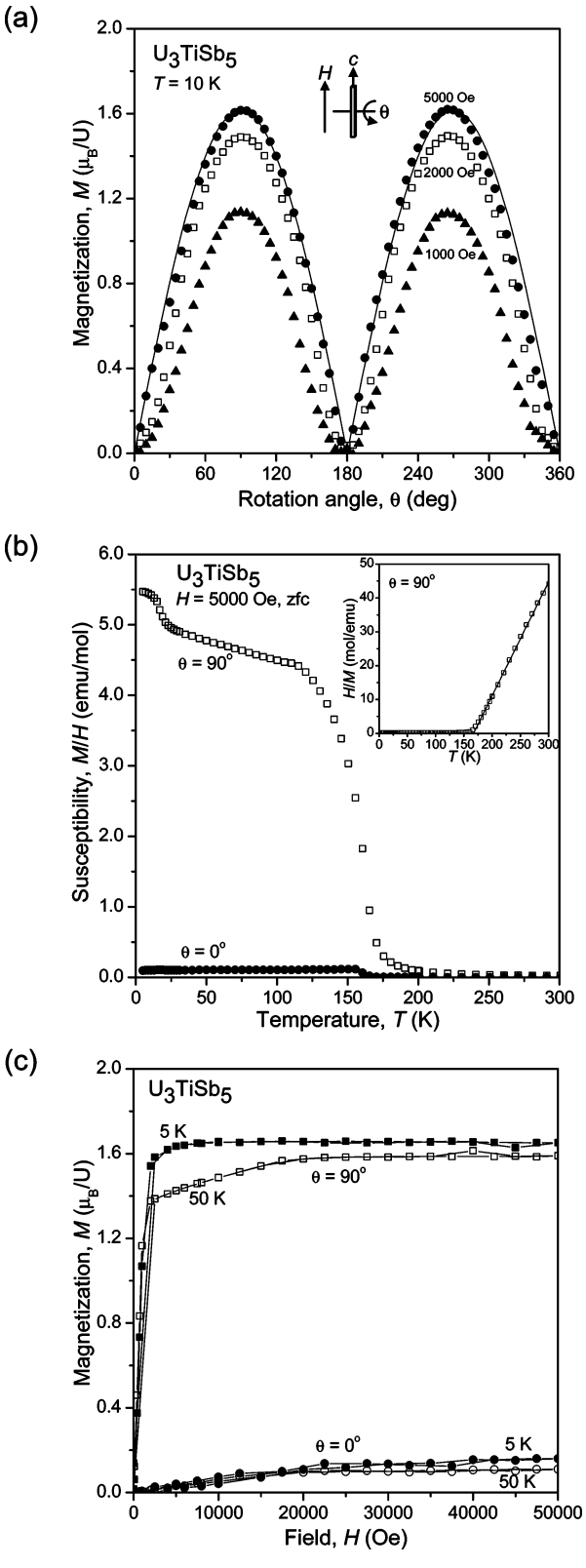

Figure 5. Magnetic properties of a single crystal of U_3TiSb_5 with the needle axis *c* rotated with respect to the applied field *H*. (a) Angular dependence of the magnetization at 10 K and under several applied fields in the range $0 < \theta < 360°$. At $\theta = 0°$ and 180°, $H \parallel c$ and at $\theta = 90°$ and 270°, $H \perp c$. The solid line is a fit to the experimental data at saturation by a sinusoidal function within 180° intervals. (b) Temperature dependence of the zero-field-cooled magnetic susceptibility at $\theta = 0°$ and $\theta = 90°$. The inset shows a fit of the inverse susceptibility data at $\theta = 90°$ to the Curie−Weiss law. (c) Field dependence of the magnetization at $\theta = 0°$ and $\theta = 90°$, at temperatures above and below the 20 K feature.

and $\theta_p = 167(1)$ K. The effective magnetic moment, $\mu_{eff} = 2.81\ \mu_B$/U, is similar to that found for U_3ScSb_5, but the higher θ_p implies stronger ferromagnetic coupling. The upturn near 25 K in the $\theta = 90°$ susceptibility curve is reproducible and appears to be a second transition. The isothermal magnetization curves (Figure 5c) reveal saturation behavior in temperature regimes above or below this 25 K transition. As before, the difference between the $\theta = 90°$ and $\theta = 0°$ magnetization curves is striking.

With the crystal remounted, the angular dependence of the in-plane magnetization was measured at a temperature below the 25 K transition (Figure 6a) and above it (Figure 6b). The curves display the expected 60° periodicity, but when the field is still low (1000 Oe), there is an additional modulation over 180°. Moreover, the evolution of the curves as the applied field is increased from 2000 to 10000 Oe (well at saturation) is different below and above this transition. At 30 K, the maxima in the magnetization curves are always at $\phi = 0°$, 60°, ..., indicating that the easy axis of magnetization is normal to the (100) faces (i.e., along the [120] direction or equivalents). However, at 10 K, there is a reversal in the positions of the maxima when the applied field exceeds 2000 Oe and up to saturation. This observation suggests that the 25 K transition may involve a spin reorientation in which the magnetic moments become aligned in a direction *between* the (100) faces (i.e., along the [100] direction or equivalents).

With the field applied along an easy magnetization axis ($\phi = 60°$), the zero-field-cooled magnetization was measured under a very low applied field of 100 Oe (Figure 6c). A plot of $d\chi/dT$ indicates the ferromagnetic ordering temperature to be $T_C = 160$ K (upper inset), and the isothermal magnetization at 5 K confirms saturation behavior (lower inset).

Electrical Properties. Plots of the electrical resistivity of single crystals of U_3ScSb_5 and U_3TiSb_5 are shown in Figure 7. In both cases, the *c*-axis resistivity (ρ_c) shows a rather weak temperature dependence in the high-temperature regime and then decreases abruptly below the onset of ferromagnetic ordering, consistent with the loss of spin-disorder scattering. For U_3TiSb_5, the resistivity undergoes an upturn at low temperature. The changes in slope are pinpointed clearly in the plots of $d\rho_c/dT$, shown in the insets. The transition temperatures identified from the resistivity curves (U_3ScSb_5, 125 K; U_3TiSb_5, 155 and 20 K) are close to the magnetic ordering temperatures determined earlier. The profiles of these curves are similar to those found previously for other U_3MSb_5 (M = Zr, Hf, Nb) compounds[6] but with slightly lower resistivity values. In contrast, the in-plane resistivity (ρ_{ab}) is marked by the absence of a transition at the ferromagnetic ordering temperature. The resistivity is nearly constant at high temperatures followed by an unusual convex curvature that flattens out abruptly below 10 K in U_3TiSb_5 but never does so in U_3ScSb_5. As well, the small values of the residual resistivity ratios (RRR = ρ_{300K}/ρ_{2K}), ranging from 1 to 3 for either the *c*-axis or in-plane resistivity, suggest that U_3ScSb_5 and U_3TiSb_5 are more appropriately classified as semimetals.

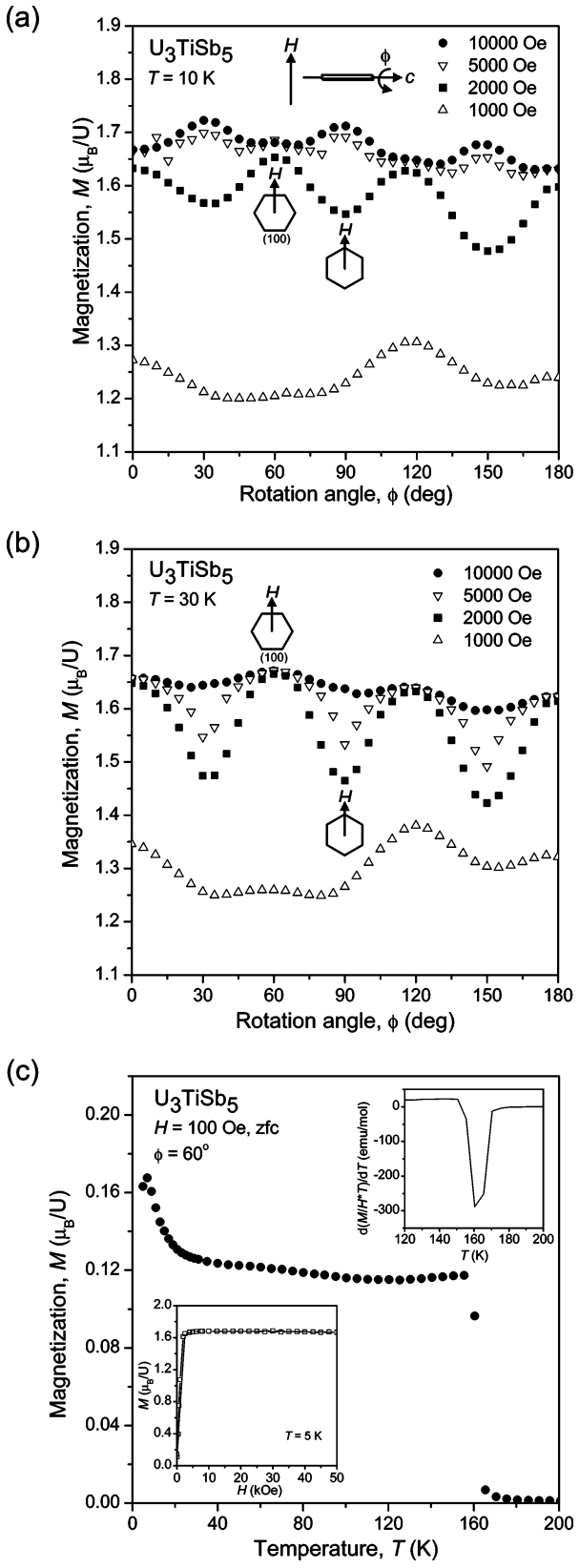

Figure 6. Magnetic properties of a single crystal of U_3TiSb_5 rotated about its needle axis *c*, oriented normal to the applied field *H*. Angular dependence of the magnetization within the *ab* plane under several applied fields in the range $0 < \phi < 180°$ at (a) 10 K and (b) 30 K. (c) Temperature dependence of zero-field-cooled magnetization under a low applied field of $H = 100$ Oe at $\phi = 90°$. The Curie temperature is determined from the plot of the derivative of $(M/H)T$, shown in the upper inset. The isothermal magnetization at 5 K is shown in the lower inset.

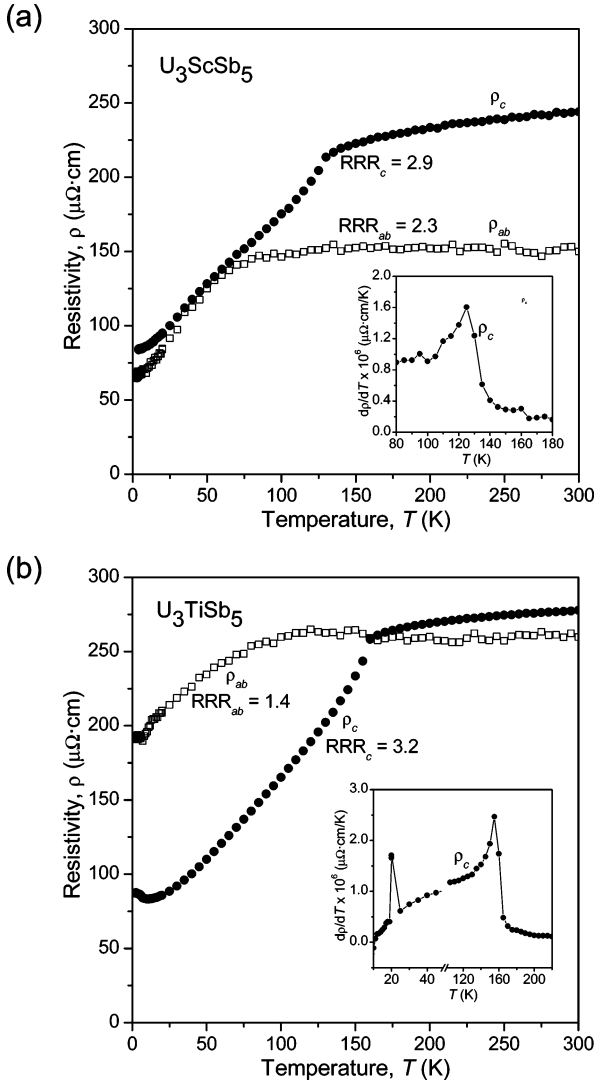

Figure 7. Electrical resistivity of single crystals of (a) U_3ScSb_5 and (b) U_3TiSb_5, measured parallel to *c* or within the *ab* plane. The insets show the derivative of ρ_c.

Because the magnetic measurements have already established these materials to be highly anisotropic, a significant difference between ρ_{ab} and ρ_c was expected. However, it is surprising to observe that the magnetic ordering has a more pronounced effect on ρ_c than on ρ_{ab}, given that the easy axis of magnetization lies within the *ab* plane and that there are essentially no magnetic interactions along the *c* direction. This seems to imply that the magnetic coupling of moments within the *ab* plane occurs through the intermediary of conduction electrons delocalized along the *c* direction. A band structure calculation for the $[TiSb_5]^{9-}$ substructure of the isostructural La_3TiSb_5 compound does indicate very high dispersion of bands in the *c* direction,[8] although how the additional orbital overlap provided by the intervening rare-earth or especially uranium atoms would modify the electronic structure remains unclear. The similarity of the absolute values of ρ_{ab} and ρ_c (Figure 7) suggests that conduction is equally facile in either direction.

Figure 8 shows the thermoelectric power measured along the *c* axis for U_3TiSb_5 and U_3ScSb_5. For U_3TiSb_5, the thermopower is positive and small at high temperatures following approximately a linear dependence with temperature in this region, indicative of metallic behavior. These thermopower values are about one order of magnitude lower compared to those of promising antimonide thermoelectric materials such as RFe_4Sb_{12}[28,29] or $Yb_{14}MnSb_{11}$.[30] In good agreement with what is observed in the resistivity measurements, the thermopower presents a kink at the ferromagnetic transition temperature; below T_C, it decreases more abruptly and goes on to negative values. This seems to indicate that the system contains more than one conduction band, where hole conduction dominates at high temperatures and electron conduction at low temperatures. For U_3ScSb_5, the thermopower is also positive at high temperatures but much smaller than for U_3TiSb_5, and a smoother departure from the linear regime can be seen at a temperature slightly higher than T_C. Nevertheless, the thermopower also changes sign around T_C, indicative of a multiband conducting system as in the case of U_3TiSb_5.

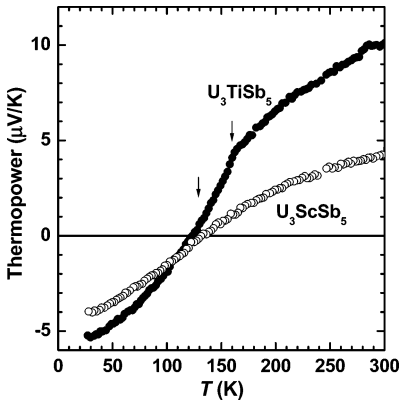

Figure 8. Temperature dependence of the thermoelectric power of single crystals of U_3TiSb_5 (closed circles) and U_3ScSb_5 (open circles), measured along the *c* axis. The arrows indicate the T_C of the ferromagnetic transitions for each compound.

Discussion

The characterization of the properties of U_3ScSb_5 and U_3TiSb_5 single crystals enables a comparison to the U_3MSb_5 (M = Zr, Hf, Nb) analogues, previously studied on powder samples.[6] As judged by their similar magnetization and resistivity profiles, all are soft ferromagnetic metals or semimetals. By inference, the identification of [120] and equivalent directions as the easy magnetization axes in U_3ScSb_5 and U_3TiSb_5 can be assumed for the other members. The coincidence of T_C in the magnetization data with a corresponding kink in the resistivity and thermopower curves points out the important role of conduction electrons in mediating the indirect exchange coupling between magnetic moments, localized on the U atoms. It is commonly recognized that the electronic properties of uranium-containing compounds are controlled by the delocalization of the 5f electrons, which can occur via either or both of two possible mechanisms: (i) direct 5f−5f overlap between wave

(28) Sales, B. C. In *Handbook on the Physics and Chemistry of Rare Earths*; Gschneidner, K. A., Jr., Bünzli, J.-C. G., Pecharsky, V. K., Eds.; Elsevier: Amsterdam, 2003; Vol. 33, pp 1−34.
(29) Nolas, G. S.; Morelli, D. T.; Tritt, T. M. *Annu. Rev. Mater. Sci.* **1999**, *29*, 89−116.
(30) Brown, S. R.; Kauzlarich, S. M.; Gascoin, F.; Snyder, G. J. *Chem. Mater.* **2006**, *18*, 1873−1877.

Table 4. Comparison of U_3MSb_5 and Related Compounds[a]

compd	av U−Sb (Å)	*M*−*M* or Sb−Sb (Å)	U−U (Å)	T_C (K)	μ_{eff} (μ_B/U)
U_3TiSb_5	3.211	3.086	3.715	160	2.81
U_3HfSb_5	3.223	3.081	3.758	141	2.18
U_3ZrSb_5	3.224	3.084	3.765	135	2.42
U_3ScSb_5	3.234	3.097	3.759	130	2.86
U_3NbSb_5	3.196	3.045	3.745	107	2.22
U_5Sb_4	3.203		3.106	86	2.98

[a] Standard uncertainties in distances are less than 0.001 Å for U_3MSb_5 and 0.005 Å for U_5Sb_4. Uncertainties are ~1 K for T_C and ~0.02 μ_B for μ_{eff} values.

functions centered on neighboring U atoms; (ii) hybridization between the uranium 5f-states and the s-, p-, or d-states of other neighboring atoms. Therefore, the magnetic parameters are expected to be governed by the U−U and U−ligand separations. In the U_3MSb_5 compounds, the shortest U−U distances (3.7−3.8 Å) well exceed the Hill limit (3.4−3.5 Å), a critical distance below which direct overlap of f orbitals on neighboring U atoms tends to obliterate magnetic ordering. Table 4 shows that the value of T_C does not follow a straightforward relationship with either U−U or other distances. Moreover, the reduction of the effective moment, by more than 20% compared to the calculated value for both f^2 and f^3 electronic configurations, indicates that the 5f−ligand hybridization is important. The detailed magnetic structure must also depend on the electron count, which modifies the position of the Fermi level in the conduction band that will be made up largely of orbital contributions from *M* or Sb atoms. Supporting this assertion, we note that U_3TiGe_5 and U_3TiSn_5 are also ferromagnetic, but the moments are aligned parallel to the *c* axis and the ordering temperatures are considerably reduced, to 76 and 65 K, respectively.[9] Although the atomic positions in U_3TiSn_5 were not refined, the closest U−U distance can be estimated to be ~3.7 Å, similar to that in the U_3MSb_5 compounds.

This situation is comparable to the hexagonal *R*PtIn and *R*AgGe compounds (ZrNiAl-type, $P\bar{6}2m$), which switch between ferromagnetic and antiferromagnetic ordering and between ordering in the axial or basal directions, depending on *R*.[19] Although the planar arrangement of *R* atoms is similar to that of the U atoms in U_3MSb_5 (anti-Hf_5Cu_3Sn-type, $P6_3/mcm$), their stacking along the *c* direction is different. Further analysis of the magnetic data for U_3MSb_5 to extract CEF parameters would be desirable, and a definitive corroboration of the magnetic structure will require neutron diffraction experiments. These results also provide motivation for investigation of other U_3MSb_5 members, which also form for M = V, Cr, and Mn,[5] to discern the trends in magnetic properties more clearly and for rigorous calculation of the electronic band structure including the U atoms.

Acknowledgment. This work was supported by the Centre National de la Recherche Scientifique of France. Additional support to A.M. was provided by the Natural Sciences and Engineering Research Council of Canada and the University of Alberta. The Université de Rennes 1 provided access to the Nonius Kappa CCD diffractometer through its Centre de Diffraction X (CDIFX).

Supporting Information Available: Crystallographic data in CIF format. This material is available free of charge via the Internet at http://pubs.acs.org.

CM061281Y